Chiral Micellar Porphyrin Fibers with 2-Aminoglycosamide Head Groups

Jürgen-Hinrich Fuhrhop,*,† Corinna Demoulin,† Christoph Boettcher,†,‡ Jürgen Köning,† and Ulrich Siggel§

Contribution from the Institut für Organische Chemie der Freien Universität Berlin, Takustrasse 3, 1000 Berlin 33, Germany, Fritz-Haber-Institut der Max-Planck-Gesellschaft, Faradayweg 4-6, 1000 Berlin 33, Germany, and Max Volmer Institut für Physikalische Chemie der Technischen Universität, Strasse des 17 Juni 135, 1000 Berlin 12, Germany.
Received October 28, 1991

Abstract: Easily accessible protoporphyrin IX 13,17-bis(glycosamides) form colloidal aqueous solutions which are stable for several months or longer. Electron micrographs show ribbons of an approximate width of 4 nm and lengths of between 20 nm (D-glucosamide) and 5 μm (D,L-mannosamide). In one case, gel chromatography was applied in order to acquire the molecular weight, which was determined to be $\geq 2 \times 10^6$ D for about 90% of the colloidal particles. The UV–vis spectra of the aqueous suspension show a Soret band which is split by about 100 nm by exciton interactions (460 and 360 nm). Circular dichroism (CD) spectra reveal complex exciton splittings. Both the absorption and CD spectra have been reproduced by simple model calculations. Fluorescence was not present in the aggregate and the aggregates did not quench the fluorescence of the added porphyrins. Two stacked face-to-face dimers with lateral shifts to half a molecule in each direction and no dipole–dipole interactions are proposed to connect to twisted ribbons by strong edge-to-edge interactions. Longevity of the aggregate solutions is traced back to the thinness of the highly curved aggregates and their low dissociation constants ($\approx 10^{-7}$–10^{-6} M).

Synthetic micellar fibers[1-3] and aqueous vesicle membranes[4-6] can organize in aqueous media to form several well-separated or specifically connected membrane lipid and aqueous solvation volumes. In synthetic systems photo- and redox-active cofactors, namely amphiphilic porphyrins,[7,8] are of interest. These porphyrins may either themselves form micellar fibers[8] or vesicles or they may be integrated into corresponding host systems. In vectorial membrane processes, such as light-induced charge separation or oxygen processing, these porphyrin assemblies may then act as multiple donors and acceptors of electrons in a defined environment.

The porphyrin macrocycle—as a unit of such assemblies—may be considered as a rigid hydrophobic box with special packing properties. The geometric dimensions of the box are 0.7 × 0.7 × 0.35 nm^3 (Figure 1). Since it has a high density of π-electrons in the large periphery and a positive hole in the central cavity, it dimerizes with a lateral shift, i.e., an electron-rich pyrrole ring of one porphyrin migrates toward the center of a partner porphyrin and stays there[9-12] (Figure 1). Extremely stable dimers are thus formed in solution[9,10,12] as well as in crystal structures[11] and probably also form the unit of higher aggregates in water.

Dimer formation should also be helpful in the formation of bilayer structures from amphiphilic porphyrins. The most important natural porphyrin, namely protoporphyrin IX[13] (**1a**), is such an amphiphile. It contains two propionic acid side chains in the lower ("southern") pyrrole rings. If one succeeded in dissolving protoporphyrin IX or an amphiphilic derivative in water, one would predict a very stable dimer in which the porphyrin units are rotated by 180° to obtain a symmetric distribution of the hydrophilic head groups. "North" and "south" would then be hydrophilic edges, "east" and "west" edges would be hydrophobic (Figure 2). Rotation of one porphyrin relative to the other should not occur.

π–π repulsion must then be overcome to allow the formation of extended edge-to-edge connected chains. One possibility is cooperative hydrogen bonding between glycosamide head groups which have been so successful in other micellar fibers.[2] Another possibility is half-neutralization of the carboxylic acid side chains, which could produce intra- and intermolecular COOH–$^-$OOC hydrogen bonds.[3] The latter has been verified: protoporphyrin indeed produces aggregates of high molecular weight in water, which split into components with short and long wavelength Soret bands,[13] when gel filtration is applied. Long-wavelength Soret bands have also been found in surface monolayers of coproporphyrin esters,[14] in vesicular solutions,[15] and in aggregates of substituted tetraphenyl porphyrins in complexes with surfactants.[16] Furthermore it has been shown that *meso*-tetraphenylporphyrin derivatives with a long alkyl side chain produce micelles and ribbons in ethanol water, which can be identified under the electron microscope. No effects on the Soret bands[8] were observed in this case. Here, we report for the first time on long lived micellar fibers made of porphyrin glycosamides with an apparently split Soret band.

Results

Syntheses. The protoporphyrin IX glycosamides were prepared from the porphyrin–formic acid mixed anhydride **1b** and 2-deoxy-2-aminopyranosides. Only totally acylated diamides **1g–j**

† Institut für Organische Chemie der Freien Universität Berlin.
‡ Fritz-Haber-Institut der Max-Planck-Gesellschaft.
§ Max Volmer Institut für Physikalische Chemie der Technischen Universität.

(1) Nakashima, N.; Asakuma, S.; Kunitake, T. *J. Am. Chem. Soc.* **1985**, *107*, 508–510.
(2) Fuhrhop, J.-H.; Schnieder, P.; Rosenberg, J.; Boekema, E. *J. Am. Chem. Soc.* **1987**, *109*, 3387–3390.
(3) Fuhrhop, J.-H.; Demoulin, C.; Rosenberg, J.; Boettcher, C. *J. Am. Chem. Soc.* **1990**, *112*, 2827–2829.
(4) Fendler, J. H. *Membrane Mimetic Chemistry*; Wiley: New York, 1982.
(5) Fuhrhop, J.-H.; Fritsch, D. *Acc. Chem. Res.* **1986**, *19*, 130–137.
(6) Ringsdorf, H.; Schlarb, B.; Venzmer, J. *Angew. Chem.* **1988**, *100*, 117–162.
(7) Fuhrhop, J.-H.; Lehmann, T. In *Optical Properties and Structures of Tetrapyrroles*; Sund, H., Blauer, G., Eds.; de Gruyter: Berlin, 1985; pp 19–42.
(8) Guilard, R.; Senglet, W.; Liu, Y. H.; Sazon, D.; Findsen, E.; Faure, D.; Des Courieres, T.; Kadish, K. M. *Inorg. Chem.* **1991**, *30*, 1898–1905.
(9) Hunter, C. A.; Sanders, J. K. M. *J. Am. Chem. Soc.* **1990**, *112*, 5525–5534.
(10) Hunter, C. A.; Sanders, J. K. M.; Stone, A. J. *Chem. Phys.* **1989**, *133*, 395–404.
(11) Scheidt, W. R.; Lee, Y. J. *Struct. Bond.* **1987**, *64*, 24–40.
(12) Smith, K. M. *Acc. Chem. Res.* **1979**, *12*, 374–381.
(13) Inamura, I.; Uchida, K. *Bull. Chem. Soc. Jpn.* **1991**, *64*, 2005–2007.
(14) Bergeron, J. A.; Glaines, G. L.; Bellamy, W. D. *J. Colloid Interface Sci.* **1967**, *25*, 97–106.
(15) van Esch, J.-H.; Peters, A.-M. P.; Nolte, J. M. *J. Chem. Soc., Chem. Commun.* **1990**, 638–639.
(16) Barber, D. C.; Freitag-Beeston, R. A.; Whitten, D. G. *J. Phys. Chem.* **1991**, *95*, 4074–4086.

0002-7863/92/1514-4159$03.00/0

Table I. Adsorption Spectra of Aqueous Solutions

	Soret 1		Soret 2		Q_4		Q_2		Q_1	
compound	λ/nm	$\epsilon/M^{-1}\ cm^{-1}$	λ/nm	ϵ	λ/nm	ϵ	λ/nm	ϵ	λ/nm	ϵ
D-Glu-P, **1c**	358	3.4×10^4	448	3.4×10^4	534	1.83×10^4	587	1.15×10^4	641	7.57×10^4
D-Man-P, **1d**	358	4.4×10^4	(445) sh	4.0×10^4	532	1.85×10^4	586	1.1×10^4	641	6.0×10^4
L-Man-P, **1e**	359	4.0×10^4	445	4.5×10^4	531	2.2×10^4	587	1.4×10^4	641	8.8×10^4
D-Gal-P, **1f**	362		451		535		591		643	

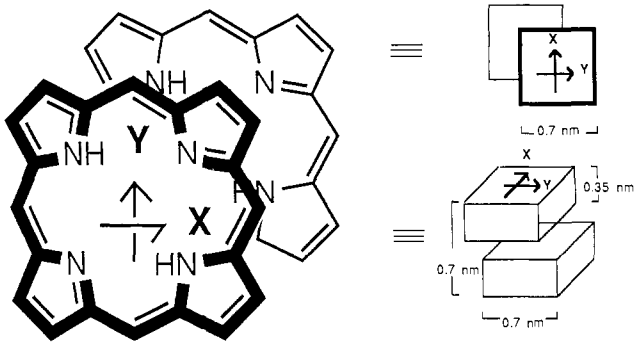

Figure 1. Optimum geometry for the porphyrin–porphyrin macrocycle interaction. The coordinate system used is also given (see discussion).

could be purified by chromatography on silica gel and were fully characterized by elemental analysis, spectroscopy (^1H and ^{13}C NMR, UV–vis, IR), and fast atom bombardment mass spectra. Deacylation with potassium hydroxide gave the protoporphyrin diamides **1c–f** containing only free hydroxyl groups.[5] These compounds were best characterized by elemental analyses and IR spectra.

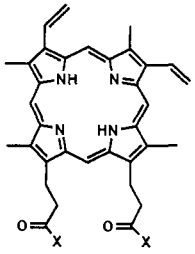

1a X = H (protoporphyrin IX)

1b X = OCH(O)OEt (mixed anhydride)

1c X = D - Glu - Proto

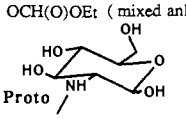

1d X = D - Man - Proto

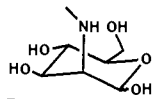

1e X = L - Man - Proto

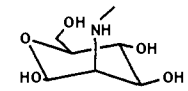

1f X = D - Gal - Proto

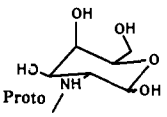

1g, h, i, j same as **1c,d,e,f**, but OAc instead of OH

1k same as **1a**, but CHOH-Me instead of vinyl (hematoporphyrin)

Split Soret Bands, Hydrogen Bonds, and Molecular Mass in Aqueous Solution. The bis(tetraacetates) **1g–j** were soluble in chloroform and produced a Soret band at 405 nm ($\epsilon = 1.5 \times 10^5\ M^{-1}\ cm^{-1}$) with a dipole strength of 189 D^2 as the sum of two degenerate Soret transitions S_x and S_y was determined.[17] It is accompanied by four Q-bands of low absorption strength at 505, 540, 575, and 629 nm. Practically identical UV–vis spectra were obtained from DMSO and micellar sodium dodecyl sulfate solutions of the free carbohydrate derivatives **1c–f**. The half-width of the Soret band was 45 ± 5 nm in all cases and its slope was much steeper on the long wavelength side. Uroporphyrin, which is the only natural porphyrin for which a monomer has clearly been demonstrated in solution,[18,19] produces a Soret band with a half-width of 30 nm. In our case, broadness and asymmetry of the Soret band are clear indications of some porphyrin aggregation, probably dimerization. There is, however, no appreciable exciton shift,[10,16,20] although the dimer must clearly be cofacial. This finding is explained on the basis of the assumptions made in the introduction, namely that the porphyrin macrocycles in the dimer are shifted in both the *x*- and *y*-directions. The vector connecting both dipole centers then has an angle close to 55° (see Figure 10) with respect to the porphyrin planes and dipolar interactions would shrink.[16] A fluorescence emission band with peaks at 631 and 696 nm was common to these solutions of dimers.

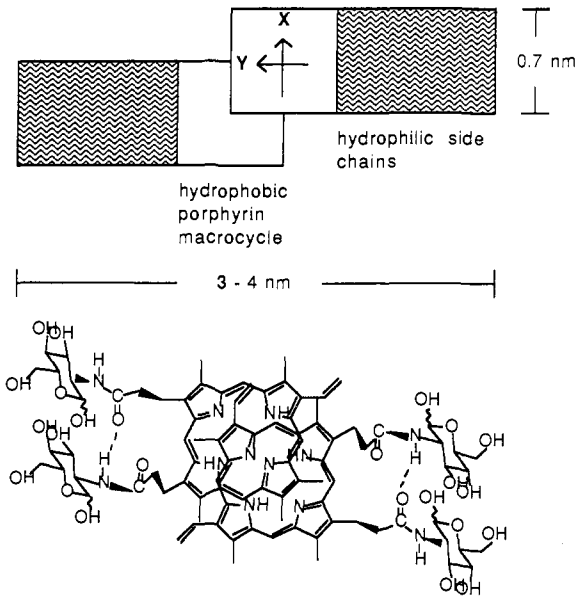

Figure 2. Optimum dimer structure of amphiphilic porphyrins (here: D-Glu-Proto **1c**).

In distilled water (at pH 6–7), the glycosamides **1c–f** dissolved up to concentrations of around 3×10^{-3} M. The *racemic mixture* of D- and L-mannosamides **1d** and **1f** (1:1) was somewhat less soluble than the pure *enantiomers*, but this could not be quantitized. The UV–vis spectra of the four compounds and of the racemate were very similar and exhibited an extremely broadened

(17) $M^2 = 3hc \cdot \epsilon / 2N_A\pi^2$, $\epsilon d\lambda/\lambda = 9(19 \times 10^{-3})$, $\epsilon(d\lambda/\lambda)[D^2]$ see, for example, Cantor, C. R.; Schimmel, R. R. *Biophysical Chemistry*; Freeman: New York 1980 (M = transition moment, D = Debye unit of dipole moment).

(18) Mauzerall, D. *Biochemistry* **1965**, *4*, 1801–1810.

(19) Shelnutt, J. A.; Dobry, M. M.; Satlerlee, J. D. *J. Phys. Chem.* **1984**, *88*, 4980–4987.

(20) Braue, E. H.; Pannella, M. G. *Appl. Spectrosc.* **1990**, *44*, 1513–1520, and references therein.

(21) Kasha, M.; El-Bayoumi, M. A.; Rhodes, W. *J. Chim. Phys.* **1961**, *58*, 916–925.

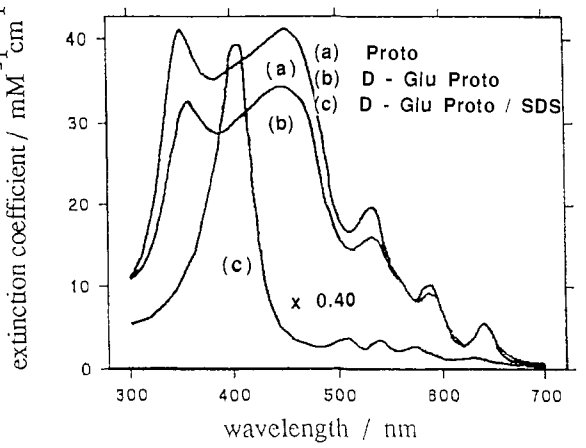

Figure 3. Absorption spectra of aqueous solutions of (a) protoporphyrin IX **1a** (pH = 7; contains 20% DMSO), (b) D-Glu-Proto **1c**, and (c) D-Glu-Proto **1c** in presence of 4% sodium dodecyl sulfate (SDS). The extinction coefficient of the SDS solution is 9×10^4 ($\lambda_{1/2}$ = 43 nm) as compared to 1.5×10^5 ($\lambda_{1/2}$ = 46 nm) in DMSO solution original concentrations: (a) 1.77×10^{-5} M; (b) 4.5×10^{-5} M; (c) 2.1×10^{-5} M.

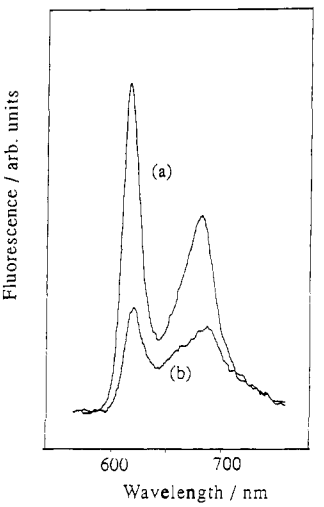

Figure 4. Fluorescence spectra (right angle excitation) of (a) 10^{-6} M hematoporphyrin **1k** in presence of 10^{-4} M D-Glu-Proto **1c** fibers and (b) of the same fibers in absence of hematoporphyrin; λ_{exc} = 380 nm.

split Soret band (Figure 3) which extended from 300 to 600 nm with maxima at 358 and 445–450 nm. The relative heights of the two Soret peaks in aqueous solution vary with the glycosamide unit. The red-shifted peak is, for example, prominent in the L-mannosamide **1e**, whereas it appears as a "shoulder" in the D-enantiomer **1d** (Table I). The Q-band region shows only three, instead of four, bands at 533, 587, and 641 nm (Figure 3). The extinction coefficients of the Soret bands are lowered by a factor of 4, if compared to the 405-nm band in organic or micellar solutions. Beer's law applies in the concentration range from 10^{-6} to 5×10^{-4} M within 5%. The fit is actually better than in organic solvents or micellar solutions. Only traces of a 405-nm peak were ever observed in aqueous suspensions at concentrations above 10^{-6} M for glucosamide **1c**. We therefore assume a large aggregate with a dissociation constant well below 10^{-6} M. Mannose- and galactosamide aggregates were somewhat more dissociated and a dissociation constant close to 10^{-6} M was estimated. The spectrum of one sample of an aqueous solution of glucosamide **1e** was measured again after a period of 9 months and had remained essentially unchanged. Increasing the temperature to 90 °C did not change the UV–vis spectra; thus the aggregate seems neither to dissociate appreciably upon dilution or heating nor to crystallize or precipitate.

The split Soret band is again replaced by a single 405-nm band upon addition of sodium dodecyl sulfate (SDS) or methylformamide (MFA). In water–MFA (molar ratio 3:1), the unsplit 405-nm Soret band becomes the prominent one. The action of SDS depends on both the concentration and time. At room temperature and 1.6% of SDS, a partial conversion of the split to the 405-nm Soret band was observed within 15 min; this then slowed down and continued for weeks. In the concentration range of (9×10^{-3})–0.35 M SDS we found higher SDS concentrations to be more effective. There was, however, no break at the critical micellar concentration of SDS, and even at 4% SDS, the split Soret band was not completely replaced by the 405-nm band.

In order to look for amide hydrogen bonds, FTIR spectra of galactosamide **1f** in DMSO and in water were measured in a CIRCLE CELL.[20] The amide I band occurred at 1663 cm^{-1} in both solvents, but amide II was at 1559 cm^{-1} in DMSO and 1506 cm^{-1} in water. This is the same shift reported for polypeptides which convert from coil conformations without amide hydrogen bonds to helical conformations with strong hydrogen bonds.[22]

Comparative chromatography on acrylamide/agarose gel with dextrane blue and proteins as standards yielded molecular weights above 2×10^6 for more than 90% of the porphyrin **1c**. The appearance of the split Soret band showed practically no changes between the unfractionated solution and the first 19 fractions containing ≥80% of the porphyrin. Only in the very last fractions does the 350-nm band become more prominent. This result is a strong argument for a largely uniform structure of the aggregates.

An attempt was also made to produce aqueous solutions of nonderivatized protoporphyrin IX with a split Soret band by variations of pH, salt concentrations, and use of cosolvents. Inamura et al. have recently reported on acid titrations and found a split Soret band at pH 4.8.[16] We have only seen spectra with a shoulder of 460 nm at pH = 7. Rapid precipitation occurred at a lower pH. Our best results were obtained by dilution of protoporphyrin IX DMSO solutions with water. Addition of 0.5 M NaCl had no effect. In the narrow range of molar ratios water/DMSO from 1:4 to 1:6, there was a change from the dimer to the aggregate spectrum which resembled a phase transition. At a ratio of 1:20, the 405-nm peak disappeared completely and the UV–vis spectrum therefore became very similar to the one in aqueous glyconamide solutions (Figure 3). Protoporphyrin aggregates are thus much less stable than those of the corresponding aminoglycosamides. The unstable protoporphyrin IX aggregates in the solvent mixture were so difficult to handle, especially in electron microscopy, that they were not further investigated.

Hematoporphyrin, which carries two α-hydroxyethyl instead of vinyl groups, is more water-soluble than protoporphyrin and has no hydrophobic edge. It may be considered as a bolaamphiphile[23] with the porphyrin macrocycle as hydrophobic core and four head groups. Its DMSO solution was also diluted with water at pH 6–7. Neither a splitting of the Soret band at 405 nm nor loss of fluorescence occurred. Franck reported water-soluble isohemato porphyrin diglycosides, which apparently did not form any aggregates either.[24]

The aqueous solution of the protoporphyrin glycosamides hardly fluoresces. Low-intensity fluorescence (see Figure 4) probably originates from some dimer dissociated from the aggregate. We then assumed that hematoporphyrin could neither penetrate into the amide hydrogen bonded protoporphyrin glucosamide aggregates nor get close to the protoporphyrin chromophores surrounded by hydrophilic glucosamide units. A 10^{-6} M hematoporphyrin solution still showed a strong fluorescence in the presence of 10^{-4} M glucosamide porphyrin **1c** (Figure 4). The 10^{-4} M solution of **1c** alone showed a fluorescence of the same intensity as a 5×10^{-7} solution of hematoporpphyrin in the presence of 10^{-4} M glucosamide porphyrin **1c**. Reabsorption of the fluorescence is about the same in both cases, because the glucosamide porphyrin

(22) Kauzmann, W. *Annu. Rev. Phys. Chem.* **1957**, *8*, 413–440.

(23) Fuhrhop, J.-H.; Fritsch, D. *Acc. Chem. Res.* **1986**, *19*, 130–137.
(24) Fülling, G.; Schröder, D.; Franck, B. *Angew. Chem.* **1989**, *101*, 1550–1552.

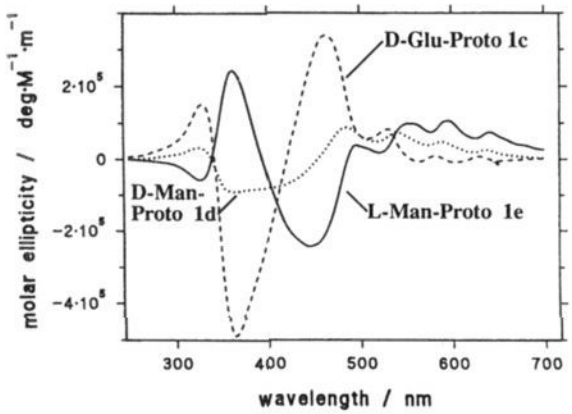

Figure 5. Circular dichroism spectra D-Glu-Proto **1c**, D-Man-Proto **1d**, and L-Man-Proto in aqueous solutions (4×10^{-5} M).

concentration is the same. It can therefore be neglected. We conclude that the dissociation constant of the aggregate is about 5×10^{-7} M. The aggregate is therefore at least a hundredfold more stable than porphyrin–nucleic acid complexes.[25] The addition of 1 M sodium chloride influenced neither the hematoporphyrin nor the protoporphyrin fluorescence and the adding of glutaraldehyde as a cross-linker of the carbohydrate head groups had only very little effect on the fiber dissociation.

Circular Dichroism and Electron Microscopy. If the amide and hydroxyl groups of the chiral carbohydrate substituents form hydrogen bonds between the porphyrin molecules, one may also expect chiral superstructures—namely helices, or twisted ribbons. It is the existence (or nonexistence) of a circular dichroitic (CD) response which gives implicit information on the angles between monomer planes in such arrangements. The DMSO solutions of all amphiphilic porphyrins **1a** and **1c–f** were CD-inactive. In contrast, the aqueous solutions gave characteristic CD spectra. The D-glucosamide **1c** shows an asymmetric positive band at 466 nm and a negative one at 364 nm. Both correspond roughly to the split Soret band of the electronic spectrum. The maximal molar ellipticity is 4.9×10^5 deg M^{-1} m^{-1}. A small band at 330 nm can also be seen and the tail of the long wavelength band is modulated by positive Q-bands. The CD spectra of D- and L-mannosamides **1d** and **1e** are of lower intensity (Figure 5); they are not strictly mirror images of each other (see Discussion). D-Mannosamide showed a large negative band which constitutes the sum of two bands with minima at 365 and 415 nm. The L-mannosamide has a CD band around 340 nm of sign opposite to that of the D-enantiomer, but of like sign in the 400–500 nm region (see Figure 5).

Addition of SDS decreases the CD amplitudes. The three main bands are sensitive to approximately the same degree. There is a good linear correlation between the relative intensities of absorption bands at 448 nm and the CD band at 330 nm (Figure 6) and the more stable aggregate of **1c** shows greater rotational strength than the less stable aggregates of **1d,e**. This is another strong argument in favor of only one dominant type of porphyrin glycosamide aggregate in aqueous solutions which produces both the red- and blue-shifted exciton Soret bands. This assumption is further strengthened by the finding that both the red- and blue-shifted Soret bands have the same half-widths of 5000 cm^{-1}.

The experimental results described so far suggest a stable, high molecular weight bilayer of the porphyrin glycosamides in water. This should be detectable by electron microscopy. The solution of **1c** in distilled water did indeed (upon evaporation on the electron microscope grid) produce many short fibers with widths between 4.0 and 6.0 nm. Their lengths varied from about 20 to 200 nm. A few thicker and longer aggregates of many such fibers were also present. At higher magnification, several of the fibers showed striations of about 1.5 nm (Figure 7a). The attempt with high-resolution image analyses unfortunately failed, because the short fibers could not be ordered to allow averaging. D,L-Mannosamide mixtures gave much longer fibers (Figure 7b), which is in agreement with the lower solubility of this racemate and may constitute another example of the chiral bilayer effect.[2,3] The structural features of the aggregates, obtained in negative

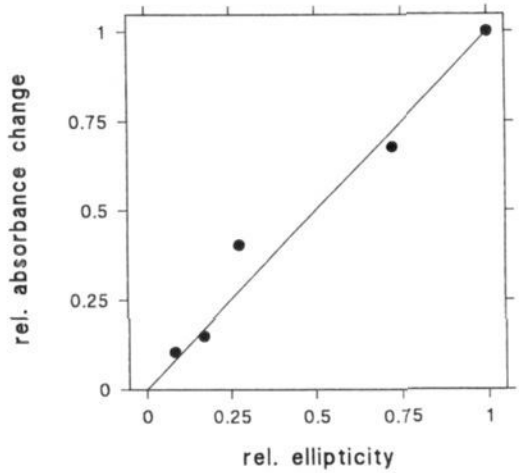

Figure 6. Correlation between the absorbance change at 448 nm and CD change at 329 nm upon addition of SDS to the aqueous solution (SDS concentration at (a) 0.25% and (b) 4%; porphyrin concentration at 4.3×10^{-5}).

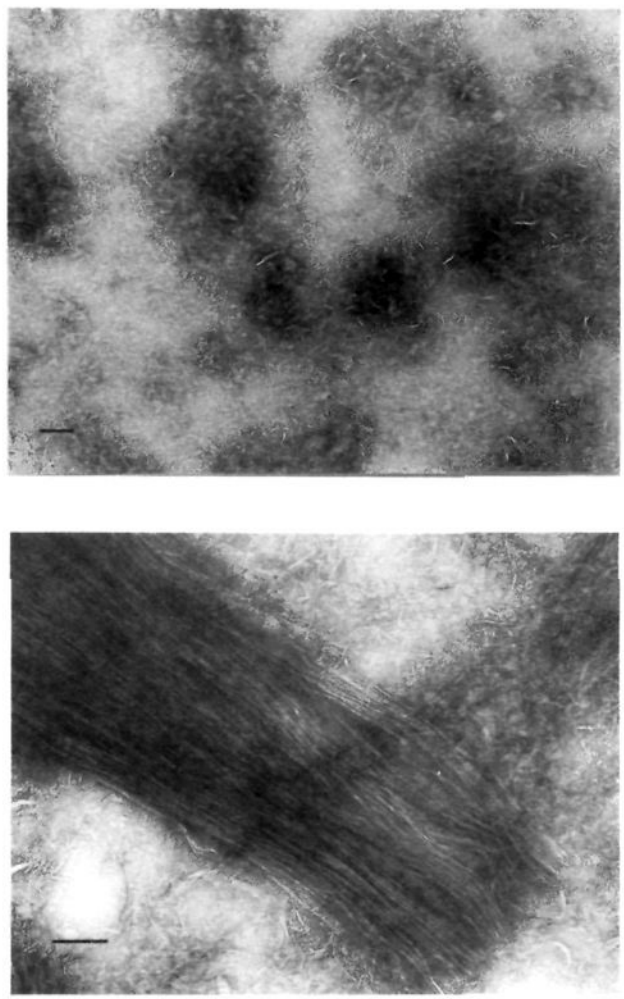

Figure 7. Electron micrograph of fibers made of (a) D-Glu-Proto **1c** (bar, 200 nm) and (b) D,L-Man-Proto **1d,e** (1:1; bar, 100 nm), negative staining, uranyl acetate.

(25) Pasternack, R. F.; Gibbs, E. J.; Villafranca, J. J. *Biochemistry* **1983**, *22*, 2406–2414.

Table II. Circular Dichroism Spectra of Aqueous Solutions

	band 1		band 2		band 3	
compound	λ/nm	[Θ]/deg M^{-1} m^{-1}	λ/nm	[Θ]	λ/nm	[Θ]
D-Glu-P, **1c**	329	$+1.51 \times 10^5$	365	-4.88×10^5	464	$+3.37 \times 10^5$
D-Man-P, **1d**	325	$+3.28 \times 10^4$	364	-9.00×10^4	486	$+8.79 \times 10^4$
L-Man-P, **1e**	327	-5.81×10^4	362	$+2.44 \times 10^5$	445	-2.44×10^5

staining preparation, were also confirmed by using the vitrified ice-embedding technique, where the staining and dehydration artifacts were absent. More detailed comparative work is, however, required in order to quantitize the fiber lengths and average molecular weights from different porphyrin amphiphiles.

Attempts to characterize the fibers by differential scanning calorimetry and solid-state cross-polarized magic angle spinning (CP-MAS) NMR spectroscopy led only to broad signals.

Discussion and Theory

Here we start with two assumptions on the porphyrin aggregates: (i) the fundamental unit of the aggregate is the dimer of a structure closely resembling the model given in Figure 2, (ii) the observed apparent Soret band splitting comes from transition dipole interactions. These assumptions and exciton model calculations—using point[10,21] and extended[26] transition dipoles—will be used to develop a structural model which reproduces the UV–vis and the more detailed CD spectra. The results of the model calculations will then be combined with other experimental data (molecular weight, electron micrographs, fluorescence, FTIR) and a final model of the porphyrin fiber will be proposed.

The experimentally found blue shift of the Soret band (3320 cm^{-1}) was always much larger than the red shift (−2520 cm^{-1}). Calculations with simple edge-to-edge arrays of dimers always produced a red shift about twice as large as the blue shift. This is true for the point dipole approximation[21] as well as for the extended dipole model.[26] The theory therefore excludes a one-way aggregate and requires a *combination* of cofacial and edge-to-edge interactions. In the first step a tetramer of dimer units (=an octamer) with only nearest neighbor interactions was calculated. In a second step an infinite number of edge-to-edge neighbors was allowed for the calculation of the first splitting, neglecting the additional energy niveaus of low intensity. For this polymer ribbon, the splitting of S_x should be double the size as for the edge-to-edge dimer. The splitting scheme with four energy levels each for S_x and S_y is shown in Figure 8. In this figure the first splitting is arbitrarily taken as due to edge-to-edge alignment. Each of the resulting levels is split a second time because of the stacking. The allowed optical transitions correspond to the levels E_1 (red-shifted Soret band S_x) and E_1' (blue-shifted Soret band S_y). A value of 0.81 is allowed for both bands and zero for the other six. The energy shifts ΔE_1 and $\Delta E_1'$ for the S_x and S_y transitions relative to the unsplit Soret band are given by

$$\Delta E_1 = -\frac{4M^2}{r_a^3} + \frac{M^2}{r_b^3} \text{ and } \Delta E_1' = \frac{2M^2}{r_a^3} + \frac{M^2}{r_b^3}$$

where r_a is the distance of transition dipole moments M for the edge-to-edge arrangements, whereas r_b is the same distance within the stacks.

The strong energy splitting of 5840 cm^{-1} of the Soret band requires a strong transition dipole of the ribbon type aggregate of porphyrins (see Figure 10a). This implies that the S_x transition dipoles of individual porphyrin molecules are in a head-to-tail position, which is only possible if they point to the methine bridges. In this case, we applied this assumption, although it is not in agreement with Gouterman's four-orbital model[27] and earlier molecular orbital models. It might be justified if one allows for configuration interaction between transitions of different symmetry. Maruyama et al. ran into the same trouble when wanting to calculate Soret band splittings in covalent pentamers.[28]

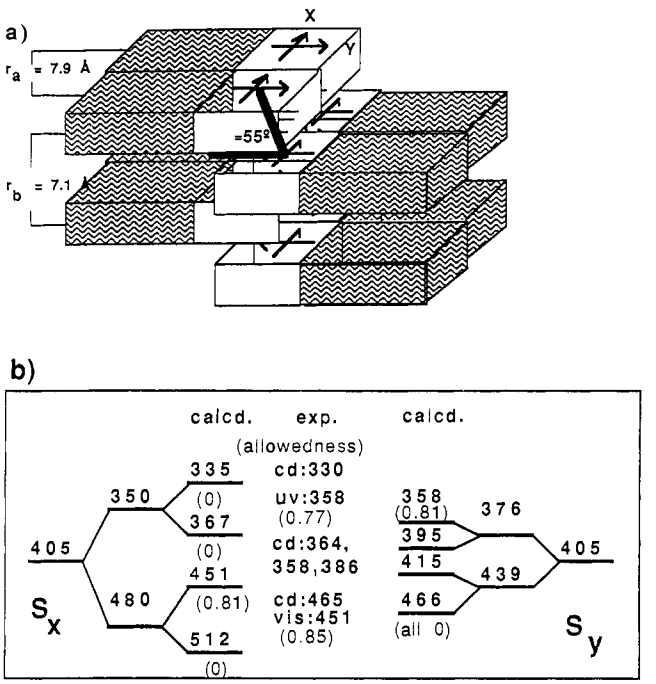

Figure 8. (a) Model of the amphiphilic octamer unit and in this model calculations (see text). The white part stands for the porphyrin macrocycle, the wavy section indicates hydrophilic glycosamide units in the assumed hydrophobic bilayer. (b) Energy splitting of the Soret band as calculated by point dipole exciton interaction from the structure given above. Calculated and experimental values for the wavelengths are in nm. The corresponding allowedness is given in parentheses.

From the experimental blue and red shifts ($\Delta E_1'$, ΔE_1), the porphyrin distances were obtained using both the point[21] and extended[26] dipole formalisms (assumed length of dipole, 0.5 nm). The distance between the porphyrin centers in edge-to-edge pairs was calculated as $r_a = 0.79$ and 0.88 nm, respectively, the distance between cofacial porphyrin dimers came out as $r_b = 0.71$ and 0.49. In view of the approximations (nearest neighbor interactions and flat instead of twisted ribbon) the discrepancy to reasonable distances (see Figure 8a) is surprisingly small. The blue- and red-shifted bands correspond to Gaussian functions of 64 and 97 nm half width. The squares of the transition moments can be calculated with Gouterman's equation to be 0.77 and 0.85. This is in excellent agreement with the calculated value of 0.81. Of more importance is the possibility to calculate the other six levels (taking r_a and r_b from the point dipole approximation) and to correlate them with the CD spectra. The differing complex CD spectra (Figure 6) have to be interpreted as a summation of four exciton band pairs of varying sign. The positions of which should correspond to the eight energy levels calculated by us. This summation leads to new extrema. Therefore the spectra of D- and L-enantiomers need not to be antisymmetric. Even without detailed analysis, several features of the complex CD spectra are immediately explained by the calculation. In particular, the calculated transition at 335 nm is optically forbidden but appears in the CD spectrum (Figure 8b).

The exciton CD spectra of the fibrous porphyrin aggregates are more complicated than the induced CD spectra shown by cationic porphyrins which adsorb to, or intercalate with, nucleic

(26) Czikklely, V.; Försterling, H. D.; Kuhn, H. *Chem. Phys. Lett.* **1970**, *6*, 207–210.
(27) Gouterman, M. *J. Mol. Spectrosc.* **1961**, *6*, 138–163.
(28) Nagata, T.; Osuka, A.; Maruyama, K. *J. Am. Chem. Soc.* **1990**, *111*, 3054–3059.

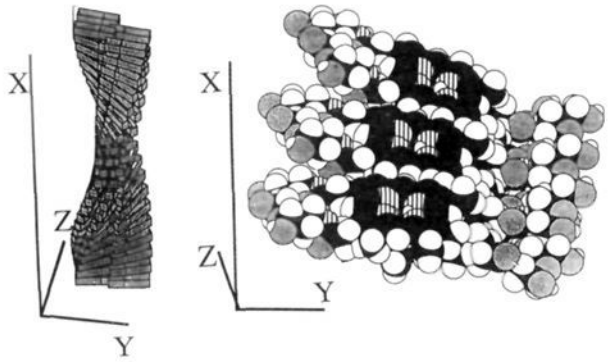

Figure 9. Computer graph of the assumed twisted polymer ribbon consisting of the octamer units and molecular model of a small section of the upper half of the polymer ribbon including the twisting.

acids.[25,29] These polymer–chromophore aggregates showed only one induced CD band at 430 nm, corresponding to the Soret band of the *meso*-tetrapyridylporphyrins investigated. The surprising lack of bands in the Q-band region of the induced CD bands was not discussed by the authors.

As a result of these considerations we propose an octameric unit of the aggregate: four dimers are packed cofacial and edge-to-edge (Figure 8b). The minimum volume of this octamer would be 8.4 nm^3; a more realistic guess would be a value close to 10 nm^3. Electron micrographs suggest fibers which are about as thick as the longest side of the elementary unit, namely 4–6 nm. The average length of a ribbon is 20–40 nm. If we assume 2 nm as a length of the octamer of 2 nm, then a 30 nm long fiber would contain $15 \times 8 = 120$ porphyrins. This gives a molecular mass of 1.1×10^5 and is by a factor of 20 smaller than that determined by gel chromatography. We assume that further aggregation of fibers takes place on the column. The electron micrographs of the D,L-mannonamide porphyrin (Figure 7) indeed show 4–6 nm fibers which are several hundred nanometers long. The fibers obviously grow in length by attaching at the hydrophobic ends. Thickness growth does not take place, which explains the observed stability of the colloidal solutions for at least several months.

A summary of the structural assignments is given in the computer drawing in Figure 9 which also reproduces the twist of ribbon suggested by the intense CD effects.

Conclusion

A major asset of the colloidal porphyrin particles is their unique longevity. They neither coagulate nor photodegrade. Furthermore, they can be mixed with dimeric, photoactive porphyrins and hardly quench their fluorescence. The porphyrin fibers can thus be envisaged as multiple acceptors or donors of electrons in interactive systems with excited states which provide energy-rich electrons and electron holes. For this purpose, the oxidation potentials of the porphyrin monomers should be varied by introduction of different metal ions. Fibers made of zinc porphyrins could, for example, be loaded with several electron holes by oxidation; tin(IV) porphyrins fibers could hold several surplus electrons. Work on this energy storage and collection device is in progress.

Experimental Section

General Methods. Melting points were determined on a Kofler apparatus (Reichert) and are uncorrected. Analytical thin-layer chromatography (TLC) was performed on alumina sheets procoated with silica gel 60 F_{254} (Merck). Column chromatography was carried out with silica gel 60 without indicator (Merck). ^1H NMR and ^{13}C NMR spectra were recorded in DMSO on a Bruker AC 250 and AM 270 SY spectrometer. All chemical shifts (δ) are reported in ppm with tetramethylsilane as internal standard. Elemental analyses were performed by the Mikrolabor der Freien Universität Berlin and Microlab Ilse Beetz, 8410 Kronach, Germany. CD spectra were obtained from a JASCO J 500 A spectrometer (Japan Spectroscopic Co.) using 1-cm and 0.1-cm cuvettes. UV–visible spectra were recorded on a DU-7 US Beckmann spectrophotometer. Electron microscopy was done at the Fritz-Haber-Institut der Max-Planck-Gesellschaft Berlin using a (Philips) and at the Institut für Elektronenmikroskopie der Freien Universität Berlin using an Elmiskop U39 (Siemens). Mass spectra were obtained from CH 5 DF, MAT 112, and MAT 7U spectrometers (Varian-MAT) with positive FAB (fast atom bombardment) method, the matrix was 3-nitrobenzoyl alcohol/DMSO and xenon as primary ion source. Circle cell IR spectra were recorded on a Nicolet 800 FTIR spectrometer.

General procedure for the synthesis of Protoporphyrin IX $13^3,17^3$-Bis(2-amido-2-desoxy-α,β-D,L-glycopyranosides 1c–f. Protoporphyrin IX (**1a**) (250 mg, 0.44 mmol) was suspended in 25 mL of dry tetrahydrofuran and 1.5 mL (10.7 mmol) of dry triethylamine. The mixture was cooled to 0 °C and 1.3 mL (13 mmol) of ethyl chloroformate was added dropwise under stirring at 0 °C. After 0.5 h the reaction was complete. TLC (chloroform–methanol (9:1)) showed a single spot of mixed anhydride **16** ($R_f = 0.9$).

A solution of 795 mg (4.4 mmol) of **2a** in 3 mL of ethanol, 1.5 mL (10.7 mmol) of triethylamine, and 0.3 mL of water was added slowly to the stirred reaction mixture and was kept for 12 h at ambient temperature. The progress of the reaction was followed by TLC. All protoporphyrin bis(glycosamides) (**1c–f**) remained at the base line with chloroform–methanol (9:1).

The solvent was removed under reduced pressure and the residue suspended in 20 mL of methanol–water (4:1). In some preparations the products were still partly soluble in this solvent mixture, which remained red. If this was the case, a few drops of 10% acetic acid was added until complete precipitation occurred. After filtration several washings with cold methanol–water (2:1) were applied to remove the excess of amino sugar. After drying, the solid was suspended in chloroform, stirred for 1 h, filtered, and washed repeatedly with chloroform until the filtrate was colorless.

The crude protoporphyrin bis(glycosamides) **1c–f** were thus obtained in 70–90% yield as black-violet solids. The raw material, e.g. 1.15 g (1.3 mmol), was dissolved in 50 mL of dry pyridine. The solution was cooled to 0 °C followed by the dropwise addition of 25 mL of acetic anhydride. The solvent was removed under vacuum and several times coevaporated with toluene–chloroform (7:3). The residual solid was chromatographed on a silica gel column (chloroform–methanol (50:1)); 70–77% of the bis(tetraacetate) **1g–j** were obtained upon removal of the solvents.

Bis(tetraacetates (**1g–j**) (756 mg, 0.62 mmol) were dissolved in 150 mL of tetrahydrofuran. Potassium hydroxide (1.14 g, 20 mmol) in 300 mL of methanol–water (1:1) was added and the reaction mixture stirred for 1 h at room temperature. In the chloroform–methanol (9:1) eluent all red compounds remained at the origin, IR spectra showed no ester bands. Tetrahydrofuran was evaporated, the remaining aqueous solution was neutralized and the precipitates were filtered off. Inorganic materials were removed by several washings first with ethanol followed by cold methanol–water (2:1). The residue was dried in vacuo: yield 70–77% **1c–f** as black-violet powders.

Protoporphyrin $13^3,17^3$-Bis(2-amido-2-desoxy-α,β-D-glucopyranose (1c): Mp 258 °C (dec). Anal. Calcd for $C_{46}H_{56}N_6O_{12}$ (884.96): C, 62.43; H, 6.38; N, 9.50. Found: C, 61.88; H, 5.83; N, 9.29. IR (KBr): 3600–3200 (OH); 3305 (ν_{NH}); 1660 (amide I); 1565 (amide II). ^1H NMR (DMSO-d_6) δ −4.18 (m, 2 H, N–H), 3.1, 4.3 (m, 8 H, 13^1, 17^1, 13^2, 17^2-CH_2); 3.5, 3.6 (m, 12 H, 2, 8, 12, 18 -CH_3); 4.1–5.05 (div. m, C–H, OH from glucose moiety), 6.18 (d, 2 H, $J = 13$ Hz), 6.39 (d, 2 H, $J = 20$ Hz, 3^2, 8^2 =CH); 8.1 (m, 2 H, amide-H); 8.39 (m, 2 H, 3^1, 8^1 -CH=); 10.12 (m, 4 H, 5, 10, 15, 20 methine-H).

Protoporphyrin $13^3,17^3$-Bis(2-amido-2-desoxy-α,β-D-mannopyranose (1d). Mp 220–232 °C (dec). Anal. Calcd for $C_{46}H_{56}N_6O_{12}$ (884.96): C, 62.43; H, 6.38; N, 9.50. Found: C, 63.03; H, 6.14; N, 9.60. IR (KBr) **1d + 1e**: 3600–3200 (OH); 3305 (ν_{NH}); 1655 (amide I); 1555 (amide II). ^1H NMR **1d** (DMSO-d_6): δ −4.27 (m, broad, N–H), 3.0–5.0 (div. m, C–H, O–H from mannose moiety); 3.59 (m, 2, 8, 12, 18-CH_3); 4.41 (m, 13^2, 17^2 -CH_2); 6.20, 6.42 (d, 4 H, 3^2, 8^2 =CH_2); 7.66 (m, 2 H, amide-H); 8.42 (m, 2 H, 3^1, 8^1 -CH=); 10.12 (m, 4 H, 5, 10, 15, 20 methine-H).

Protoporphyrin $13^3,17^3$-bis(2-amido-2-desoxy-α,β-L-mannopyranose (1e). Mp 220–232 °C (dec). Anal. Calcd for $C_{46}H_{56}N_6O_{12}$ (884.96): C, 62.43; H, 6.38; N, 9.50. Found: C, 62.12; H, 6.37; N, 9.15.

Protoporphyrin $13^3,17^3$-Bis(2-amido-2-desoxy-α,β-D-galactopyranosid (1f). Mp 256 °C (dec). Anal. Calcd for $C_{46}H_{56}N_6O_{12}$ (884.96): C, 62.43; H, 6.38; N, 9.50. Found: C, 62.26; H, 6.27; N, 9.15. IR (KBr): 3600–3200 (OH); 3305 (ν_{N-H}); 1640 (amide I); 1535 (amide II) cm^{-1}. CC-IR: (DMSO) 1661 (amide I); 1559 (amide II) cm^{-1}; (water) 1665 (amide I); 1506 (amide II) cm^{-1}. ^1H NMR (DMSO-d_6) δ −4.0 (m, 2 H, N–H); 2.62–5.0 (div. m, C–H, O–H from galactose moiety); 3.72 (*s* ≈ 12 H, 2, 8, 12, 18 -CH_3); 4.36 (*m* ≈ 4 H, 13^2, 17^2 -CH_2); 6.23, 6.42

(29) Gibbs, E. J.; Tinoco, I.; Maestre, M. F.; Ellinas, A. E.; Pasternack, R. F. *Biochem. Biophys. Res. Commun.* **1988**, *157*, 350–358.

(d, 4 H, 3^2, 8^2 =CH); 8.5 (m, 2 H, 3^1, 8^1 CH=); 10.19 (m, 4 H, 5, 10, 15, 20 methine-H).

Protoporphyrin 13^3,17^3-Bis(1,3,4,6-tetra-*O*-acetyl-2-amido-2-desoxy-α,β-D-glucopyranose) (1g). Mp 156 °C (dec). Anal. Calcd for $C_{62}H_{72}N_6O_{20}$ (1221.25): C, 60.97; H, 5.94; N, 6.88. Found: C, 61.03; H, 5.95; N, 6.90. IR (KBr): 3310 (ν_{N-H}); 1750 ($\nu_{C=O}$); 1685 (amide I); 1530 (amide II) cm^{-1}; 1225 (st C–O acetate) cm^{-1}. ^1H NMR (DMSO-d_6): δ −4.0 (s, 2 H, N–H); 1.75–2.15 (div. acetyl-CH_3); 3.2, 4.36 (m, 8 H, 13^1, 17^1, 13^2, 17^2 –CH_2); 3.65 (s, 12 H, 2, 8, 12, 18 –CH_3); 3.93–5.18 (div. m, C–H from glucose moiety); 5.7 (1-Hβ); 5.88 (d, 1-H_α, $J_{1,2}$ = 2.7 Hz; 6.2 (d, 2 H, J = 12 Hz), 6.4 (d, 2 H, d = 19 Hz, 3^2, 8^2 =CH); 8.15 (m, 2 H, amide N–H); 8.5 (m, 2 H, 3^1, 8^1 –CH=); 10.15 (m, 4 H, 5, 10, 15, 20 methine-H). ^{13}C NMR (DMSO-d_6): δ 13.84, 12.18, 11.03 (pyrrole-CH_3); 19.26, 19.44, 20.05, 20.15, 20.27, 21.04, 21.31, 21.66 (acetyl-CH_3); 36.41 (propyl-CH_2); 59.77 (glu C-2); 61.27 (glu C-6); 68.03, 68.86, 69.51 (glu C-4, C-5, C-3); 89.59 (glu C-1); 96.31, 96.48, 96.75, 97.01 (meso-C); 120.49, 129.84, (CH=CH_2); 135.67–143.26 (div. pyrrole-C); 168.57–171.71 (div. C=O); 172.29, 172.33 (C=O propyl). MS + FAB/xenon: m/e 1221 $[M]^+$ (7%); calcd 1221.25.

Protoporphyrin 13^3,17^3-Bis(1,3,4,6-tetra-*O*-acetyl-2-amido-2-desoxy-α,β-D-mannopyranose (1h). Mp 209 °C (dec). Anal. Calcd for $C_{62}H_{72}N_6O_{20}$ (1221.25): C, 60.97; H, 5.94; N, 6.88. Found: C, 61.32; H, 6.11; N, 7.15. IR (KBr): 3310 (ν_{N-H}); 1750 ($\nu_{C=O}$); 1685 (amide I); 1530 (amide II); 1225 (st C–O, acetyl) cm^{-1}. ^1H NMR (DMSO-d_6): δ −4.06 (s, 2 H, H–H); 1.87–2.12 (s, div. acetyl-CH_3); 3.18, 4.38 (m, 8 H, 13^1, 17^1, 13^2, 17^2 –CH_2); 3.61 (m, 12 H, 2, 8, 12, 18 –CH_3); 3.94, 4.55, 4.74, 5.24, 5.48, 5.55, 5.77 (div. m, C–H from mannose moiety), 5.85 (d, 1-Hα, $J_{1,2}$ = 2.7 Hz); 6.18 (d, 2 H, J = 12 Hz and 6.44 (d, 2 H, J = 19 Hz, 3^2, 8^2 =CH); 8.45 (m, 4 H, amide N–H, 3^1, 8^1 –CH=); 10.18 (m, 4 H, 5, 10, 15, 10 methine-H). ^{13}C NMR (DMSO-d_6): δ 11.23, 12.40, 14.48 (pyrrole-CH_3); 17.60, 19.45, 19.81, 20.02, 20.29, 20.41, 20.61, 21.83 (acetyl-CH_3); 37.88 (propyl-CH_2); 96.72 (meso-C); 120.70, 129.99 (CH=CH_2); 135.96–139.53 (div. pyrrole-C); 167.78–169.90 (div. C=O); 172.8 (propyl C=O). MS + FAB/xenon m/e 1161 $[M - OAc]^+$ (1.1%); calcd 1221.25.

Protoporphyrin 13^3,17^3-Bis(1,3,4,6-tetra-*O*-acetyl-2-amido-2-desoxy-α,β-L-mannopyranose (1i). Mp 210 °C (dec). IR (KBr): 3310 (ν_{N-H}); 1750 ($\nu_{C=O}$); 1685 (amide I); 1530 (amide II); 1225 (st C–O acetyl) cm^{-1}. ^1H NMR (DMSO-d_6): δ −4.24 (m, 2 H, N–H); 1.83–2.17 (s, div. acetyl-CH_3); 3.17, 4.37 (m, 8 H, 13^1, 17^1, 13^3, 17^2 –CH_2); 3.64 (m, 12 H, 2, 8, 12, 18 –CH_3); 3.99, 4.55, 4.74, 5.15, 5.44, 5.52, 5.80, 5.85 (div. m, C–H from mannose moiety); 6.17 (d, 2 H, J = 12 Hz) and 6.41 (d, 2 H, J = 19 Hz, 3^2, 8^2 =CH); 8.43 (m, 4 H, amide N–H, 3^1, 8^1 –CH=); 10.12 (m, 4 H, 5, 10, 15, 20 methine-H). MS + FAB/xenon m/e 1221 $[M]^+$ (5.45%); calcd 1221.25

Protoporphyrin 13^3,17^3-Bis(1,3,4,6-tetra-*O*-acetyl-2-amido-2-desoxy-α,β-D-galactopyranose (1j). Mp 214 °C (dec). Anal. Calcd for $C_{62}H_{72}N_6O_{20}$ (1221.25): C, 60.97; H, 5.94; N, 6.88. Found: C, 61.57; H, 5.99; N, 7.53. IR (KBr): 3310 (ν_{N-H}); 2990–2920 (ν_{C-C}); 1750 ($\nu_{C=O}$); 1685 (amide I); 1530 (amide II); 1225 (st C–O, acetyl) cm^{-1}. ^1H NMR (DMSO-d_6): δ −4.12 (s, 2 H, N–H); 1.82–2.29 (s, div. acetyl-CH_3); 3.06, 4.29 (m, 8 H, 13^1, 17^1, 13^2, 17^2 –CH_2); 4.00 (m, 4 H, 6a,b-H from galactose moiety); 4.76, 5.04, 5.07, 5.23, 5.67, 6.0 (m, div. C–H from galactose moiety); 6.24 (d, 2 H, J = 12 Hz) and 6.48 (d, 2 H, J = 19 Hz, 3^2, 8^2 =CH), 8.21 (m, 2 H, amide N–H); 8.48 (d d, 2 H, 31.81 –CH=); 10.18 (m, 4 H, 5, 10, 15, 20 methine-H). MS + FAB/xenon: m/e 1161 $[M - OAc]^+$ (2.63%); calcd 1221.25.

Gel Chromatography. Gel chromatography of an aqueous protoporphyrin gluconamide (**1**) solution was performed as follows: One milliliter of the sample solution (3×10^{-4} M; pH = 6.5) was applied onto a column (2.0 × 30 cm) of AcA 22 (Serra, acrylamide/agarose (2%/2%)) gel. This was eluted with buffer (50 mM Tris/HCl, 100 mM KCl, pH = 7.5) at a flow rate of 8 mL/h. As molecular mass references we used the MW-GF-1000 kit (Sigma) which contains polymers in the molecular mass range from 3×10^4 D (carbonic anhydrase) to 2×10^6 D (Dextran). The content of the porphyrin fractions (1–28; 2.35 mL each) were analyzed by UV–vis spectroscopy. Most of the porphyrin (≥80%) was in fractions 5–16. All of these fractions contained porphyrin aggregates with a molecular mass of 2×10^6 or above and showed a spectrum very similar to the unfractionated solution (see Figure 5). The last fractions containing less than 5% of the total porphyrin showed only a short wavelength peak at about 370 nm and molecular mass around 6×10^5.

Preparation of Aqueous Solutions. **1c** (0.46 μg, 0.5×10^{-3} mmol) was dissolved in 5.2 mL of water (millipore quality). Clear, red solutions were obtained for the protoporphyrin bis(glycosamides) (**1c–f**). Stock solutions (10^{-4} M) showed only small deviations in the UV–vis spectra over a period of 3 months. For **1c** the ratio of the red absorption to the blue absorption changed from 1.04 to 1.08, **1d** changed from 0.86 to 0.94, and **1e** changed from 1.08 to 1.14. The position of the maxima did not change at all within a period of 3–9 months.

Electron Microscopy. Droplets of the aqueous solution of **1c** or **1d,e** (1:1) were placed onto carbon-coated copper grids (400 mesh), and after 30 s, excess fluid was blotted off. The remaining thin film of the sample was contrasted for 30 s with 5 μL of 1% uranyl acetate. After removal of the excess fluid, the grids were left to air-dry. Preparations stained with 1% phosphotungstic acid (pH = 7) as a stain gave identical qualitative results but less contrast and resolution. The grids were observed in a Philips CM12 electron microscope at an acceleration voltage of 100 kV and direct magnification of 22000 (Figure 9a) and 45000 (Figure 9b) with an approximate underfocus of 4–5 Scherzer units. To avoid structural alterations by excessive electron beam/specimen interaction, the images were recorded under "low dose" conditions as was available with the microscope. Thus, the electron dose on the aggregates could be reduced down to approximately 100 electrons/$Å^2$·s.

Acknowledgment. This work has been supported by the Deutsche Forschungsgemeinschaft (SFB 312 "Vectorial Membrane Processes"), the Förderungskommission der Freien Universität, and the Fonds der Chemischen Industrie.